Tumor and Stem Cell Biology

Cancer Research

Optical Redox Ratio Differentiates Breast Cancer Cell Lines Based on Estrogen Receptor Status

Julie Hanson Ostrander[1], Christine M. McMahon[2], Siya Lem[1], Stacy R. Millon[2], J. Quincy Brown[2], Victoria L. Seewaldt[1], and Nimmi Ramanujam[2]

Abstract

Autofluorescence spectroscopy is a powerful imaging technique that exploits endogenous fluorophores. The endogenous fluorophores NADH and flavin adenine dinucleotide (FAD) are two of the principal electron donors and acceptors in cellular metabolism, respectively. The optical oxidation-reduction (redox) ratio is a measure of cellular metabolism and can be determined by the ratio of NADH/FAD. We hypothesized that there would be a significant difference in the optical redox ratio of normal mammary epithelial cells compared with breast tumor cell lines and that estrogen receptor (ER)–positive cells would have a higher redox ratio than ER-negative cells. To test our hypothesis, the optical redox ratio was determined by collecting the fluorescence emission for NADH and FAD via confocal microscopy. We observed a statistically significant increase in the optical redox ratio of cancer compared with normal cell lines ($P < 0.05$). Additionally, we observed a statistically significant increase in the optical redox ratio of ER(+) breast cancer cell lines. The level of *ESR1* expression, determined by real-time PCR, directly correlated with the optical redox ratio (Pearson's correlation coefficient = 0.8122, $P = 0.0024$). Furthermore, treatment with tamoxifen and ICI 182,870 statistically decreased the optical redox ratio of only ER(+) breast cancer cell lines. The results of this study raise the important possibility that fluorescence spectroscopy can be used to identify subtypes of breast cancer based on receptor status, monitor response to therapy, or potentially predict response to therapy. This source of optical contrast could be a potentially useful tool for drug screening in preclinical models. *Cancer Res; 70(11); 4759–66. ©2010 AACR.*

Introduction

Fluorescence microscopy is a useful tool to characterize the metabolic properties of normal and cancerous cells and tissue (1, 2). The primary oxidation-reduction (redox) reactions in cells to generate energy in the form of ATP are the conversion of NAD^+ to its reduced form NAD(P)H (henceforth referred to as NADH) and the oxidation of flavin adenine dinucleotide (FAD) to $FADH_2$, a process known as oxidative phosphorylation. Both NADH and FAD are autofluorescent and have distinct excitation and emission maxima. The optical redox ratio can be determined by calculating the ratio of the measured fluorescence intensities of NADH and FAD (NADH/FAD; ref. 3).

Alterations in cellular metabolism are an important hallmark of carcinogenesis (4). Cancer cell metabolism is often shifted from oxidative phosphorylation to aerobic glycolysis as the primary generator of cellular ATP. Although the exact mechanisms for the switch to aerobic glycolysis and altered cellular metabolism are variable and complex (4, 5), it presents clear advantages for tumor growth. These advantages include resistance to fluctuations in the local oxygen concentration (6) and alterations in the tumor microenvironment that support tumor cell migration and invasion (7, 8). This shift, which gives rise to enhanced production of lactate in the presence of high oxygen, has long been known as the "Warburg effect" (9). In aerobic glycolysis, glucose is metabolized into two pyruvate molecules, which are then converted into lactate. This results in the production of two molecules of ATP and two NADH. During oxidative phosphorylation, one molecule of glucose is converted to carbon dioxide and water, resulting in the production of 30 to 36 ATP molecules and the oxidation of 10 NADH molecules to NAD^+. Thus, the switch from oxidative phosphorylation to aerobic glycolysis results in a net increase in NADH.

Estrogens and estrogen receptors (ER) have been shown to play a role in numerous aspects of cellular metabolism in a number of organ systems, including the liver, pancreas, brain, muscle, and breast (10, 11). Estrogens/ER have been shown to increase glucose transport and glycolysis (12–15). For example, estrogen exposure has been shown to increase the expression of a number of glucose transporter (GLUT) proteins (12, 15, 16). Estrogen (but not the ER antagonist tamoxifen) increased glucose uptake and lactate production in MCF-7 xenografts as measured by C^{13} nuclear magnetic resonance imaging (13). Additionally, estrogens/ER regulate

Authors' Affiliations: [1]Department of Medicine, Division of Medical Oncology, Duke University Medical Center and [2]Department of Biomedical Engineering, Fitzpatrick Institute for Photonics, Duke University, Durham, North Carolina

Corresponding Author: Julie H. Ostrander, Duke University Medical Center, DUMC, Box 2628, MSRB 215, Durham, NC 27710. Phone: 919-668-2457; Fax: 919-668-2458; E-mail: julie.ostrander@duke.edu.

doi: 10.1158/0008-5472.CAN-09-2572

gene expression of proteins involved in the citric acid cycle and oxidative phosphorylation (10). Although not specifically studied in the breast, estrogen/ER have been shown to regulate citrate synthase, aconitase, and isocitrate dehydrogenase (17–20). Notably, isocitrate dehydrogense activity results in the reduction of NAD^+ to NADH, which is expected to cause an increase in the optical redox ratio. Furthermore, ER has been shown to localize to the mitochondria in a variety of cell types (10), and it has been proposed that mitochondrial localization of ER is important for the transcriptional regulation of numerous mitochondrial DNA–encoded genes.

Previous studies have shown that the optical redox ratio is statistically different between cancer and normal epithelial cells, with cancer cells exhibiting higher redox ratios (2, 3, 21, 22). For example, in a study comparing normal keratinocytes to human papillomavirus (HPV)–transformed cells, the authors found that HPV-transformed cells had a higher overall intensity of NADH and a lower overall intensity of FAD, which resulted in a statistically significant difference in the optical redox ratio (22). However, the optical redox ratio of NADH to FAD has not been quantified for different biological subtypes of breast cancer, nor has its relationship to breast cancer ER status been assessed.

Based on previously published reports in the literature, our primary hypotheses tested in this study were that the optical redox ratio can differentiate between malignant and nonmalignant breast cells and between ER(+) and ER(−) breast cancer cell lines. A secondary hypothesis is that the optical redox ratio can specifically monitor response to antiestrogen therapies. To test our hypotheses, we determined the optical redox ratio using a confocal microscopy approach. NADH and FAD intensities were acquired from a panel of normal mammary epithelial and breast cancer cell lines following excitation at 351 and 488 nm, respectively. The optical redox ratio differentiated normal mammary epithelial cells from breast cancer cells and also stratified breast cancer cell lines based on ER expression, which was associated with an increased optical redox ratio. Further, treatment of ER(+) breast cancer cell lines with antiestrogens resulted in a decrease in the optical redox ratio. This effect was not observed in ER(−) cell lines.

ER has proved to be a successful target of antitumor therapy in ER(+) breast tumors. However, resistance to antiestrogen therapies is a serious clinical problem for the treatment of breast cancer. Whereas ER expression is a good predictor of response to antiestrogen therapies, not all ER(+) tumors respond to therapy and some develop resistance after initially responding to therapy. Therefore, the optical redox ratio may serve as an important biomarker to differentially identify ER(+) breast cancers and monitor response to antiestrogen therapy, with applications in drug discovery and screening as well as clinical assessment of response to antiestrogen therapies.

Materials and Methods

Cell culture and reagents

MCF-10A, MDA-231, MDA-435, MDA-468, BT-20, BT-474, MDA-361, MCF-7, T47D, and ZR-75-1 cells were obtained from either the American Type Culture Collection or the Duke Cell Culture Facility. Primary human mammary epithelial cells (HMEC) were obtained from Lonza and transduced with a retrovirus encoding human telomerase catalytic subunit (hTERT). Cells that incorporated hTERT were selected with puromycin and resistant cells were pooled and used for subsequent experiments. All cell lines except MCF-10A and HMEC were cultured in minimal essential medium α (Invitrogen) supplemented with 5% fetal bovine serum, 10 mmol/L HEPES (Invitrogen), 1× nonessential amino acids (Invitrogen), 1× sodium pyruvate (Invitrogen), 1 μg/mL insulin (Invitrogen), 1 μg/mL hydrocortisone (Sigma Aldrich), and 10 ng/mL epidermal growth factor (EGF; Sigma Aldrich). MCF-10A and HMEC were cultured in MEBM (Lonza) containing insulin, EGF, hydrocortisone, and bovine pituitary extract. All cell lines were tested for *Mycoplasma* contamination at the time of purchase and all experiments were done within 6 months of purchasing cell lines.

Confocal microscopy

For all experiments testing the optical redox ratio, cells were plated at 1×10^5 per 35-mm glass-bottomed dish (MatTek Corporation). For the panel of normal mammary epithelial cells and breast cancer cell lines, cell images were obtained approximately 48 hours later on a Zeiss LSM 410 confocal microscope (Duke University Light Microscopy Core Facility). NADH intensity images were obtained by excitation at 351 nm with a Coherent Enterprise II UV laser and the emission collected with a 400-nm LP filter. FAD intensity images were obtained by excitation at 488 nm with an Omnichrome KrAr laser and the emission collected with a 505-nm LP filter. Settings for NADH were gain = 9,611, offset = 411, and for FAD, gain = 9,555, offset = 490; the pinhole was set at 1,488 μm for both NADH and FAD. The pinhole, gain, and offset remained the same for every experiment. A model cell line, MCF-10A, was imaged during each experiment to confirm that the laser power and instrument settings were comparable from day to day (internal control). For cells treated with the antiestrogens tamoxifen (Tam) or ICI 182,780 (ICI; Sigma Aldrich), cells were plated as described above, and then approximately 24 hours later, cells were treated with 2 μmol/L Tam, 100 nmol/L ICI, or vehicle control (ethanol or DMSO). Images were acquired approximately 48 hours following treatment. Each cell line was imaged on at least 2 separate days. For each imaging session, there were two plates of each cell line and two fields of view (320 μm × 320 μm) for both NADH and FAD. All images were acquired with a 40× oil objective. Each image was line averaged 16 times, and image acquisition took approximately 16 seconds. Following data collection, the NADH/FAD ratio (a measure of the reduction-oxidation ratio) was calculated for every cell in each image. For each acquired NADH and FAD image, ImageJ software (NIH, ref. 23) was used to obtain the integrated intensity of NADH and FAD for each cell in the image after the background fluorescence was subtracted. NADH values were divided by the FAD value for each cell in an image and the average NADH/FAD was calculated for the entire image ($n = 1$). All images ($n \geq 8$) were then averaged to determine the optical redox ratio.

Table 1. Summary of cell line data

Cell line	Normal vs cancer	ER status	Plates imaged	No. of images (*n*)
MCF-10A	Normal	–/low	18	36
HMEC	Normal	–/low	4	8
	Total normal		22	44
MDA-231	Cancer	Negative	5	10
MDA-435	Cancer	Negative	5	10
MDA-468	Cancer	Negative	4	8
BT-20	Cancer	Negative	4	8
	Total ER(–)		18	36
BT-474	Cancer	Positive	6	12
MDA-361	Cancer	Positive	6	12
MCF-7	Cancer	Positive	6	12
T47D	Cancer	Positive	4	8
ZR-75-1	Cancer	Positive	4	8
	Total ER(+)		26	52

RNA isolation, cDNA synthesis, and quantitative real-time PCR

To test for *ESR1* expression, total RNA from normal mammary epithelial cells and breast cancer cell lines (two independent cultures from each cell line) was isolated using the RNeasy Mini Kit (Qiagen) according to the manufacturer's instructions. On-column DNase digestions were done to eliminate any genomic DNA contamination using the RNase-Free DNase Set (Qiagen). Total RNA quantity and quality were determined using the NanoDrop ND-1,000 full-spectrum UV/Vis spectrophotometer V3.1.2. All of the RNA that was used in this study had a 260:280 ratio between 2.1 and 2.2. RNA integrity was analyzed using the Experion RNA HighSens Analysis Kit (Bio-Rad), which confirmed the

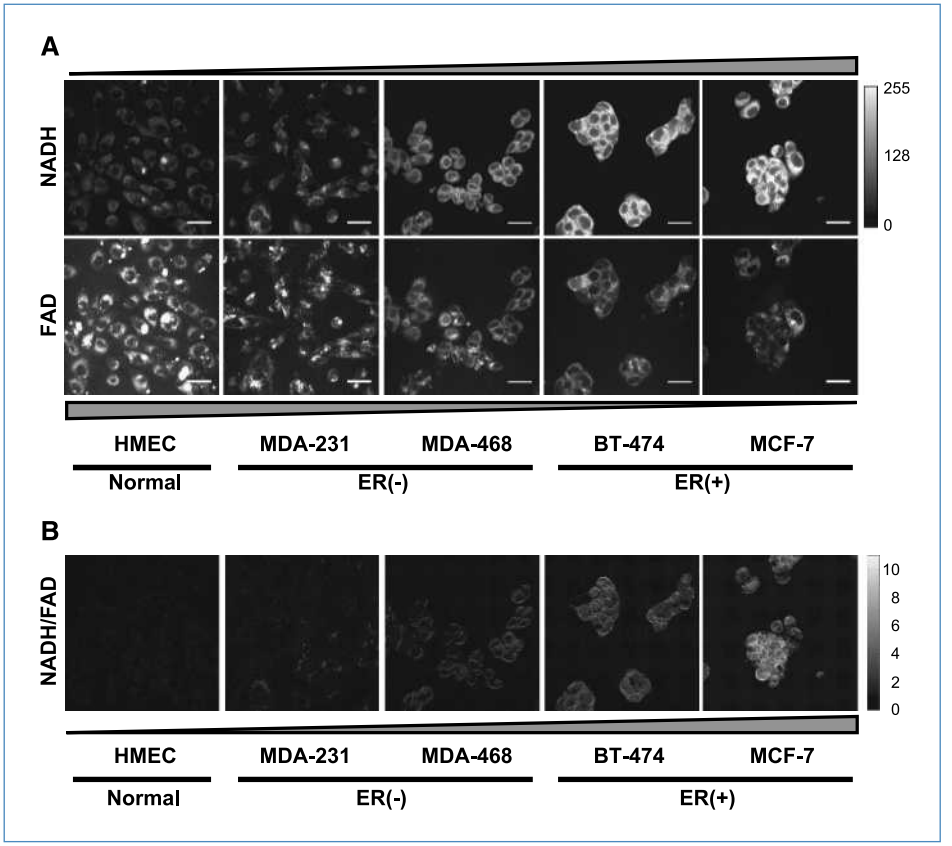

Figure 1. NADH and FAD images from breast cancer cell lines. A, representative NADH and FAD images from normal mammary epithelial cells (HMEC), ER(–) breast cancer cell lines (MDA-231 and MDA-468), and ER(+) breast cancer cell lines (BT-474 and MCF-7). Bar, 50 μm. B, redox ratio images corresponding to representative images in A, computed by dividing NADH images by FAD images pixel by pixel. The color scale (shown at the right of the figure) was optimized for MCF-7 cells and was kept constant for all images to allow direct visual comparison of redox ratio images across cell lines.

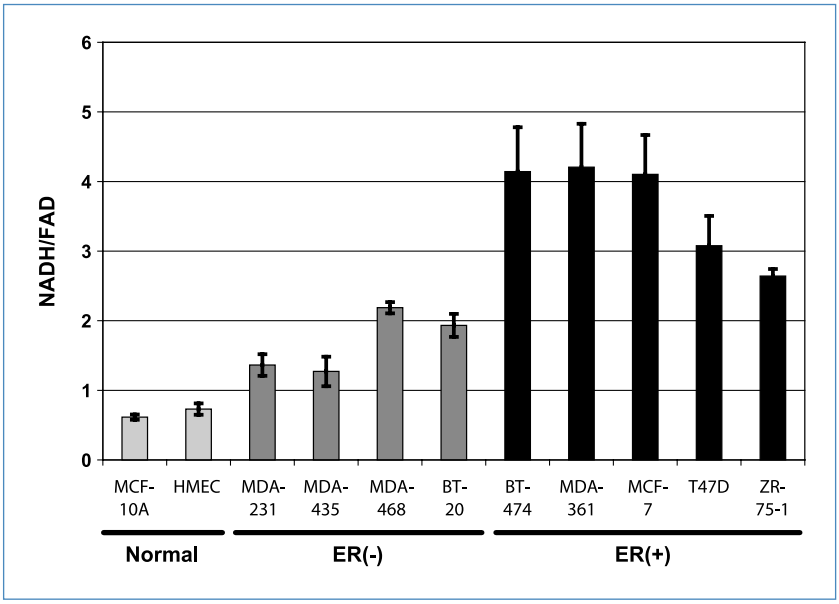

Figure 2. Optical redox ratio differentiates breast cancer cell lines. Optical redox ratio (NADH/FAD) of individual cell lines from a panel of normal mammary epithelial and breast cancer cell lines. Cell lines are grouped by normal mammary epithelial cells (light gray columns), ER(–) breast cancer cell lines (medium gray columns), and ER(+) breast cancer cell lines (black bars). Bars, SE.

presence of intact 18S and 28S rRNA. First-strand cDNA was synthesized from total RNA using the SuperScript III First-Strand Synthesis System for reverse transcription-PCR (RT-PCR; Invitrogen) according to the manufacturer's protocol.

cDNA was amplified using the QuantiTect SYBR Green PCR master mix (Qiagen) on a Bio-Rad iCycler MyiQ Single-Color Real-time PCR Detection System. *ESR1* amplification conditions were 95°C for 15 minutes, followed by 40 cycles of 95°C for 30 seconds, 58°C for 30 seconds, and 72°C for 30 seconds. 18S amplification conditions were identical except for an annealing temperature of 53°C. *ESR1* primer sequences were generated using VectorNTI software (Invitrogen): *ESR1*-F, 5′-CAGCTGTCGCCTTTCCTGCA-3′; *ESR1*-R, 5′-CACCCTGGCGTCGATTATCT-3′; 18S primers were purchased from Qiagen (QT00199367). Temperature gradients were performed to ensure that the annealing temperature for each gene was optimal. Melting curve analysis was done at the end of the PCR reaction to confirm that only one amplified product was detected. PCR amplification data were analyzed with the MyiQ Optical System Software version 1.0 (Bio-Rad). The baseline cycles and threshold were automatically calculated by the software. Because the standards were defined for each of the experimental runs, the software adjusted the threshold to attain the highest possible correlation coefficient value for the PCR standard curve. Quantitative RT-PCR was done at least twice on each cDNA from two independent RNA samples from each cell line.

Cell cycle analysis

To confirm that Tam treatment of MCF-7 cells resulted in cell cycle arrest and/or apoptosis, MCF-7 cells were plated at 2.5×10^5 per well in a six-well plate. Twenty-four hours after plating cells, triplicate wells were treated in with 2 μmol/L Tam or vehicle control for 48 hours. Cells were collected following trypsinization, washed twice with 1× PBS, and then fixed in 75% ethanol overnight. Before staining, ethanol-fixed cells were washed twice with 1× PBS. Samples were then incubated in fluorescence-activated cell sorting (FACS) staining buffer containing 1× PBS, 1 mg/mL RNase A, 0.5 μmol/L EDTA, 0.1% Triton X-100, and 100 μg/mL propidium iodide before FACS cell cycle analysis. Each experiment was repeated at least twice.

Results

Optical redox ratio differentiates breast cancer from normal cell lines

A number of previous reports suggested that the optical redox ratio (NADH/FAD) could be used to differentiate breast cancer cell lines from normal mammary epithelial cells (24, 25). To further test this hypothesis, we examined a panel of nine breast cancer cell lines and two cell line models of normal mammary epithelial cells. As described in Materials and Methods, each cell line was imaged on at least 2 separate days, two plates per cell line and two images per plate, for a minimum $n = 8$ (Table 1). MCF-10A cells, a model of normal mammary epithelial cells, were imaged each day and had a very consistent redox ratio with a small SE. Qualitatively, NADH intensity was lower and FAD intensity was higher in normal mammary epithelial cells compared with ER(–) and ER(+) breast cancer cell lines. As shown in Fig. 1A, the NADH intensity dramatically increased in ER(+) BT-474 and MCF-7 cells compared with HMEC, MDA-231, and MDA-468 cells, and FAD intensity decreased in MDA-231, MDA-468, BT-474, and MCF-7 cells compared with HMEC. Furthermore, when the NADH images were divided pixel by pixel by the FAD images, there was a dramatic increase in the NADH/FAD signal in ER(+) BT-474 and MCF-7

cells compared with HMEC, MDA-231, and MDA-468 cells (Fig. 1B).

Following ImageJ analysis, all data for each cell line were averaged, and the results are shown in Fig. 2A. We found that the optical redox ratios of MCF-10A and HMEC lines, models of normal mammary epithelial cells, were not statistically different from each other (Student's t test, $P > 0.05$), but both MCF10A and HMEC lines had statistically different optical redox ratios when compared individually to all cancer cell lines (Student's test, $P < 0.05$). Additionally, all of the ER(+) cells had higher optical redox ratios relative to all of the ER (−) breast cancer cell lines. A Tukey-Kramer test was done to account for multiple comparisons and unequal group sizes and indicated that ER(−) and ER(+) cell lines were significantly different when data were grouped as normal mammary epithelial cells, ER(−), or ER(+).

Optical redox ratio correlates with *ESR1* expression

The results from the data presented in Figs. 1 and 2 suggest that the optical redox ratio is associated with ER expression in the breast cancer cell lines. Therefore, the ER mRNA (*ESR1*) expression levels were tested by quantitative RT-PCR to determine the association between *ESR1* expression and the optical redox ratio. Total RNA was harvested from each cell line and cDNA was prepared. Quantitative RT-PCR was then performed with primers specific to *ESR1* and *18S*. All *ESR1* data were normalized to *18S*. As shown in Fig. 3A, very low expression of *ESR1* was observed in both normal mammary epithelial cell lines and all four breast cancer cell lines previously reported to be ER(−), whereas all five breast cancer cell lines previously reported as ER(+) expressed significant amounts of *ESR1*. Interestingly, we observed low *ESR1* expression in MDA-468 and BT-20 breast cancer cell lines. These two ER(−) breast cancer cell lines had statistically significant higher redox ratios than the other two ER(−) breast cancer cell lines (MDA-231 and MDA-435; Student's t test, $P < 0.05$). To determine if *ESR1* expression positively correlated with the optical redox ratio, a Pearson's correlation test was performed. We found that *ESR1* expression and the optical redox ratio were positively correlated (Pearson's correlation coefficient = 0.8122, $P = 0.0024$), further suggesting that ER expression has an effect on the optical redox ratio.

Antiestrogens modulate the optical redox ratio

Because ER expression positively correlated with the optical redox ratio, the next logical step was to test the effects of the antiestrogens Tam and ICI on the optical redox ratio. First, the effects of Tam treatment were tested by cell cycle analysis. Tam (2 μmol/L) or vehicle control was added to the normal growth medium of triplicate cultures of MCF-7 for 48 hours. MCF-7 cells were then trypsinized and fixed in 75% ethanol overnight. Samples were then stained with propidium iodide and analyzed by flow cytometry for cell cycle distribution. After 48 hours of Tam treatment, there was a statistically significant increase in MCF-7 cells with sub-G_1 content of DNA (3.6% to 7.0%; $P < 0.0001$), indicative of apoptosis, an increase in cells in the G_1 phase of the cell cycle (53% to 64%; $P = 0.0007$), and a decrease in cells in S-phase and G_2-M (S-phase: 25% to 17%, $P = 0.0007$; G_2-M: 19% to 13%, $P = 0.0017$) as shown in Fig. 4A. The cell cycle analysis indicated that 2 μmol/L Tam has a significant effect on the proliferation and cell cycle distribution of MCF-7 cells. Similar results were also obtained for MCF-7 cells treated with 100 nmol/L ICI (data not shown).

To test for Tam-induced changes in the optical redox ratio, ER(+) MCF-7 and T47D cells were treated for 48 hours with 2 μmol/L Tam or vehicle control, and NADH and FAD autofluorescence were measured as described above. Tam treatment resulted in a statistically significant decrease in the optical redox ratio in both MCF-7 and T47D breast cancer

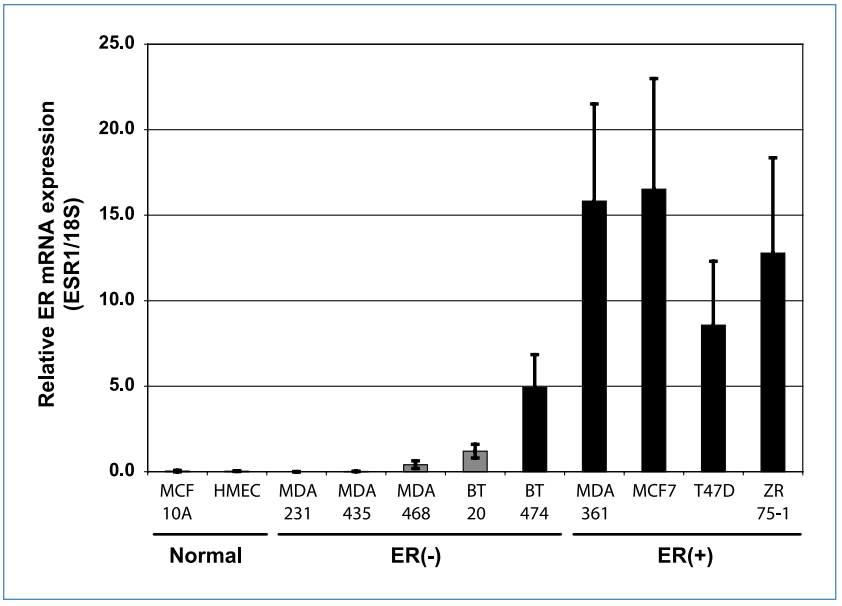

Figure 3. Optical redox ratio correlates with ESR1 expression. Quantitative RT-PCR data from normal mammary epithelial and breast cancer cell lines. All ESR1 expression data were normalized to *18S* levels in the same sample. Data presented are the average of four independent quantitative RT-PCR reactions from two separate RNA extractions for each cell line. Bars, SD.

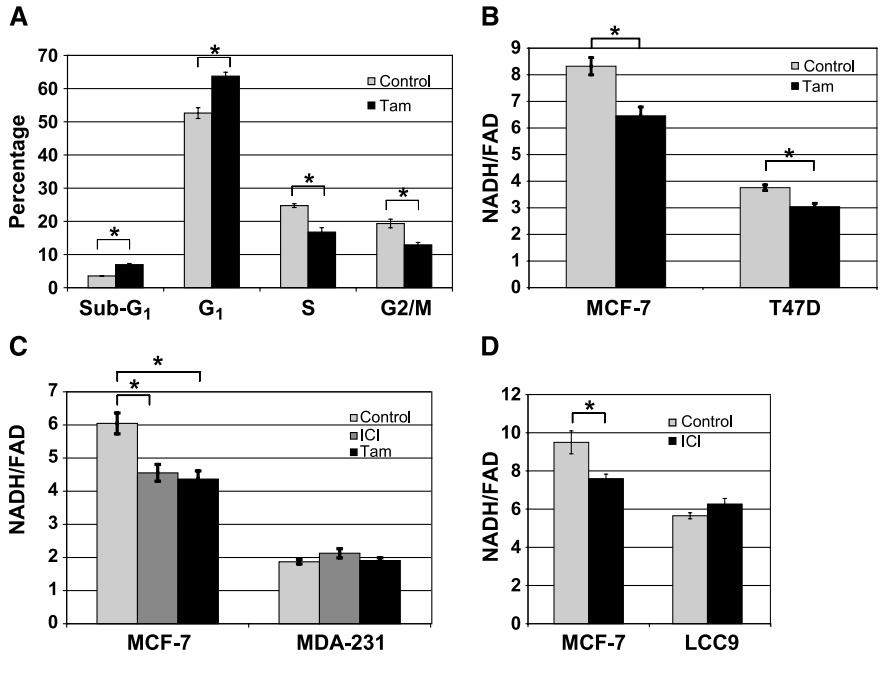

Figure 4. Antiestrogens modulate the optical redox ratio. A, flow cytometry cell cycle analysis from propidium iodide–stained vehicle control (EtOH)– and Tam-treated (48 h) MCF-7 cells. Bars, SD; *, $P < 0.05$ (Student's t test). B, optical redox ratio from ER(+) MCF-7 and T47D cells treated with vehicle control or 2 μmol/L Tam for 48 h. C, optical redox ratio was measured from vehicle control– (light gray columns), ICI- (medium gray columns), and Tam-treated (black columns) ER(+) MCF-7 and ER(–) MDA-231 cells. D, optical redox ratio was measured from parental MCF-7 cells and MCF-7–derived LCC9 cells (Tam-resistant, ICI-resistant) treated with 100 nmol/L ICI for 48 h. B to D, bars, SE; *, $P < 0.05$ (Student's t test).

cell lines (Student's t test, $P < 0.05$; Fig. 4B). Next, the effects of Tam and ICI on ER(+) MCF-7 and ER(–) MDA-231 cells were tested. The underlying hypothesis was that if the optical redox ratio is dependent on ER signaling, then the optical redox ratio of MCF-7 cells treated with Tam or ICI would decrease. However, the optical redox ratio of ER(–) MDA-231 cells would remain unchanged. Indeed, both Tam and ICI had a statistically significant effect on the optical redox ratio of MCF-7 cells (Student's t test, $P < 0.05$), but not MDA-231 breast cancer cells, as shown in Fig. 4C.

An MCF-7 variant cell line, LCC9, was also acquired from Robert Clarke at Georgetown University (26). The LCC9 cells are ER(+) but resistant to Tam and ICI. Parental MCF-7 and LCC9 cells were treated with either vehicle control or 100 nmol/L ICI for 48 hours. ICI-treated parental MCF-7 cells had a statistically significant lower optical redox ratio compared with vehicle control–treated MCF-7 cells (Student's t test, $P < 0.05$), whereas the optical redox ratio of LCC9 cells was not significantly affected by ICI treatment (Fig. 4D). Together, the data in Fig. 4 suggest that ER antagonists reduce the optical redox ratio in ER(+) breast cancer cells, but not in ER(–) or antiestrogen-resistant cell lines.

Discussion

Our study shows that the optical redox ratio (*a*) differentiates normal mammary epithelial cells from a panel of breast cancer cell lines (Fig. 2), (*b*) positively correlates with ER expression (Fig. 3), and (*c*) can be used to monitor response to antiestrogen therapy (Fig. 4).

This is the first study to examine the optical redox ratio in a panel of cell lines that includes both normal mammary epithelial cells and ER(+) and ER(–) breast cancer cell lines. Similar to our findings (Fig. 1A), a number of studies have found that NADH intensity is higher in cancer cells and high-grade dysplasia compared with normal tissue or cell lines (24, 25, 27). In a study of 35 suspected cervical lesions and 7 cases of Barrett's esophagus, higher NADH fluorescence was observed in high-grade dysplastic lesions compared with nondysplastic tissue (27). Another study, which compared one breast cancer cell line and one normal mammary epithelial cell line, found that NADH intensity was 1.8-fold higher in the breast cancer cell line (25). Interestingly, a third study found that whereas breast cancer tissue had elevated NADH compared with normal tissue, the opposite was true for oral cancers (24), suggesting that transformation-induced changes in the optical redox ratio may be specific to organ site.

Contrary to the results presented here, in a previous study by our group, NADH and FAD intensities were examined independently in MCF-10A, T47D, MDA-231, and in control and R-Ras transformed cell lines (28). This study used fluorescence spectroscopy of cell suspensions, and a statistically significant difference in NADH or FAD intensity between malignant and nonmalignant cells was not observed. One explanation for the differences in findings between our current monolayer and previous cell suspension studies is likely due to the fact that fluorescence intensity of cells in suspension is prone to random error not present in monolayer studies. Specifically, the effects of scattering from cell suspended in media can randomly attenuate or increase the fluorescence. Further, whereas NADH and FAD intensity values

provide a measure of the metabolic state, the ratio of NADH and FAD is a more robust measurement in that it provides an internal control for cell density and instrument throughput variations.

The effect of ER expression on the optical redox ratio is not surprising. As stated above, estrogens and ERs have been shown to play a role in numerous aspects of cellular metabolism (10). The results presented here further indicate the importance of estrogen/ER in cancer cell metabolism. Based on previous reports (12–15), the dramatic increase in the optical redox ratio is likely due to an increase in glucose transport and aerobic glycolysis, which results in an increase in NADH. Considering the plethora of metabolic pathways estrogens/ERs have been shown to participate in, this is likely not the whole story. Future cell culture studies may provide insight into the molecular mechanisms underlying estrogen/ER–induced effects on the optical redox ratio.

Although our study is the first to demonstrate that the optical redox ratio can be used to monitor response to antiestrogen therapy, our results are consistent with a previous study which showed that the optical redox ratio is modulated in response to the chemoprevention agent *N*-4-(hydroxyphenol)-retinamide (4HPR) in bladder and ovarian cancer cell lines (21). In the study by Kirkpatrick and colleagues, fluorescence spectroscopy was used to measure NADH and FAD intensities. Samples were excited from 270 to 700 nm to generate excitation-emission matrices from cells in suspension. NADH intensity was calculated from the excitation at 350 nm with emission wavelengths 445 to 455 nm. FAD intensity was calculated from the excitation at 450 nm with emission wavelengths 530 to 540 nm. This study, which measured the optical redox ratio as FAD/(FAD+NADH), showed a dose-dependent increase in the optical redox ratio of cells treated with 4HPR, which correlated with a significant decrease in NADH intensity. Furthermore, cell lines that exhibited a greater response to 4HPR, as assessed by cell cycle analysis, also showed an increase in the optical redox ratio. Together, our studies suggest that the optical redox ratio is a good biomarker to differentially identify ER(+) breast cancer cells and to monitor response to antiestrogen therapies. Additional studies in cell lines will allow us to further test the mechanism of ER-induced effects on the optical redox ratio. A better understanding of how ER regulates cellular metabolism may lead to additional targets for more effective therapies and for prevention of resistance to antiestrogens.

If, as our data suggest, ER has a profound effect on the optical redox ratio, our cell line data should be recapitulated in mouse models *in vivo*. We have already begun to implement fiber-optic based fluorescence spectroscopy to measure optical redox ratios in small animal models. In a recent study, we noninvasively measured hemoglobin saturation and the optical redox ratio in response to carbogen breathing in a mouse tumor model (29). Quantitative optical spectroscopy measurements of hemoglobin saturation were consistent with invasive measurements of pO_2 using an OxyLite partial oxygen pressure sensor, suggesting that noninvasive optical techniques have the potential to reliably measure changes in tumor physiology. Importantly, in individual animals there was a strong linear correlation between hemoglobin saturation and the redox ratio following the administration of carbogen, reflecting the expected relationship between redox ratio and hemoglobin saturation (oxygen demand and supply). In conclusion, optical technologies are available to measure the optical redox ratio as well as other relevant parameters, such as hemoglobin oxygenation, *in vivo*. Thus, this parameter, which has been shown to have significance in our cell study, can be translated to measurements in small animal models and ultimately in patients.

Disclosure of Potential Conflicts of Interest

No potential conflicts of interest were disclosed.

Grant Support

Department of Defense Breast Cancer Research Program Multidisciplinary Postdoctoral Award (J.H. Ostrander) and an Era of Hope Scholar Award (N. Ramanujam).

The costs of publication of this article were defrayed in part by the payment of page charges. This article must therefore be hereby marked *advertisement* in accordance with 18 U.S.C. Section 1734 solely to indicate this fact.

Received 07/09/2009; revised 12/10/2009; accepted 03/24/2010; published OnlineFirst 05/11/2010.

References

1. Breslin TM, Xu F, Palmer GM, Zhu C, Gilchrist KW, Ramanujam N. Autofluorescence and diffuse reflectance properties of malignant and benign breast tissues. Ann Surg Oncol 2004;11:65–70.
2. Skala MC, Riching KM, Gendron-Fitzpatrick A, et al. *In vivo* multiphoton microscopy of NADH and FAD redox states, fluorescence lifetimes, and cellular morphology in precancerous epithelia. Proc Natl Acad Sci U S A 2007;104:19494–9.
3. Chance B, Schoener B, Oshino R, Itshak F, Nakase Y. Oxidation-reduction ratio studies of mitochondria in freeze-trapped samples. NADH and flavoprotein fluorescence signals. J Biol Chem 1979;254:4764–71.
4. Kroemer G, Pouyssegur J. Tumor cell metabolism: cancer's Achilles' heel. Cancer Cell 2008;13:472–82.
5. Brandon M, Baldi P, Wallace DC. Mitochondrial mutations in cancer. Oncogene 2006;25:4647–62.
6. Pouyssegur J, Dayan F, Mazure NM. Hypoxia signalling in cancer and approaches to enforce tumour regression. Nature 2006;441:437–43.
7. Izumi H, Torigoe T, Ishiguchi H, et al. Cellular pH regulators: potentially promising molecular targets for cancer chemotherapy. Cancer Treat Rev 2003;29:541–9.
8. Walenta S, Wetterling M, Lehrke M, et al. High lactate levels predict likelihood of metastases, tumor recurrence, and restricted patient survival in human cervical cancers. Cancer Res 2000;60:916–21.
9. Warburg O. On the origin of cancer cells. Science (New York, NY) 1956;123:309–14.
10. Chen JQ, Brown TR, Russo J. Regulation of energy metabolism pathways by estrogens and estrogenic chemicals and potential implications in obesity associated with increased exposure to endocrine disruptors. Biochim Biophys Acta 2009;1793:1128–43.
11. Duckles SP, Krause DN, Stirone C, Procaccio V. Estrogen and

mitochondria: a new paradigm for vascular protection? Mol Interv 2006;6:26–35.
12. Cheng CM, Cohen M, Wang J, Bondy CA. Estrogen augments glucose transporter and IGF1 expression in primate cerebral cortex. FASEB J 2001;15:907–15.
13. Furman E, Rushkin E, Margalit R, Bendel P, Degani H. Tamoxifen induced changes in MCF7 human breast cancer: *in vitro* and *in vivo* studies using nuclear magnetic resonance spectroscopy and imaging. J Steroid Biochem Mol Biol 1992;43:189–95.
14. Kostanyan A, Nazaryan K. Rat brain glycolysis regulation by estradiol-17β. Biochim Biophys Acta 1992;1133:301–6.
15. Welch RD, Gorski J. Regulation of glucose transporters by estradiol in the immature rat uterus. Endocrinology 1999;140:3602–8.
16. Macheda ML, Rogers S, Best JD. Molecular and cellular regulation of glucose transporter (GLUT) proteins in cancer. J Cell Physiol 2005; 202:654–62.
17. Beckett T, Tchernof A, Toth MJ. Effect of ovariectomy and estradiol replacement on skeletal muscle enzyme activity in female rats. Metabolism 2002;51:1397–401.
18. Pastorelli R, Carpi D, Airoldi L, et al. Proteome analysis for the identification of *in vivo* estrogen-regulated proteins in bone. Proteomics 2005;5:4936–45.
19. Stirone C, Duckles SP, Krause DN, Procaccio V. Estrogen increases mitochondrial efficiency and reduces oxidative stress in cerebral blood vessels. Mol Pharmacol 2005;68:959–65.
20. Yadav RN. Isocitrate dehydrogenase activity and its regulation by estradiol in tissues of rats of various ages. Cell Biochem Function 1988; 6:197–202.
21. Kirkpatrick ND, Zou C, Brewer MA, Brands WR, Drezek RA, Utzinger U. Endogenous fluorescence spectroscopy of cell suspensions for chemopreventive drug monitoring. Photochem Photobiol 2005;81: 125–34.
22. Mujat C, Greiner C, Baldwin A, et al. Endogenous optical biomarkers of normal and human papillomavirus immortalized epithelial cells. Int J Cancer 2008;122:363–71.
23. Software IJ. [cited; Available from: http://rsb.info.nig.gov/ij].
24. Uppal A, Gupta PK. Measurement of NADH concentration in normal and malignant human tissues from breast and oral cavity. Biotechnol Appl Biochem 2003;37:45–50.
25. Yu Q, Heikal AA. Two-photon autofluorescence dynamics imaging reveals sensitivity of intracellular NADH concentration and conformation to cell physiology at the single-cell level. J Photochem Photobiol 2009;95:46–57.
26. Brunner N, Boysen B, Jirus S, et al. MCF7/LCC9: an antiestrogen-resistant MCF-7 variant in which acquired resistance to the steroidal antiestrogen ICI 182,780 confers an early cross-resistance to the nonsteroidal antiestrogen tamoxifen. Cancer Res 1997;57: 3486–93.
27. Georgakoudi I, Jacobson BC, Muller MG, et al. NAD(P)H and collagen as *in vivo* quantitative fluorescent biomarkers of epithelial precancerous changes. Cancer Res 2002;62:682–7.
28. Palmer GM, Keely PJ, Breslin TM, Ramanujam N. Autofluorescence spectroscopy of normal and malignant human breast cell lines. Photochem Photobiol 2003;78:462–9.
29. Palmer GM, Viola RJ, Schroeder T, Yarmolenko PS, Dewhirst MW, Ramanujam N. Quantitative diffuse reflectance and fluorescence spectroscopy: tool to monitor tumor physiology *in vivo*. J Biomed Optics 2009;14:024010.